CHAPTER VI

EFFECTS OF CRYSTALLINE AND ORIENTATIONAL MEMORY PHENOMENA ON ISOTHERMAL BULK CRYSTALLIZATION AND SUBSEQUENT MELTING BEHAVIOR OF POLY(TRIMETHYLENE TEREPHTHALATE)

Pitt Supaphol,* Phornphon Srimoaon, and Anuvat Sirivat

The Petroleum and Petrochemical college, Chulalongkorn University, Soi Chula 12, Phyathai Road, Pathumwan, Bangkok 10330, THAILAND

ABSTRACT

The effects of crystalline and orientational memory phenomena on subsequent isothermal crystallization and subsequent melting behavior of poly(trimethylene terephthalate) (PTT) were investigated by studying the effect of prior melt-annealing temperature T_f on subsequent isothermal crystallization kinetics, crystalline structure, and subsequent melting behavior of neat and sheared PTT samples. On partial melting, choices of the T_f used to melt the samples played an important role in determining their bulk crystallization rates, in which the bulk crystallization rate parameters studied were all found to decrease monotonically with increasing T_f. The decrease in the values of these rate parameters with T_f continued up to a critical T_f value (i.e., ca. 275°C for neat PTT samples and ca. 280°C for PTT samples which were sheared with shear rates of 92.1 and 245.6 s^{-1}). Choices of the T_f used to melt neat PTT samples had no effect on the crystal structure formed. The subsequent melting behavior suggested that the T_f used to melt both neat and sheared samples had no effect on the peak positions of the melting endotherms observed and that the observed peak values of these endotherms for all sample types studied were almost identical.

(**Key-words**: poly(trimethylene terephthalate); crystalline memory phenomenon)

* To whom correspondence should be addressed (Fax: +66-2215-4459, E-mail address: pitt.s@chula.ac.th)

1. INTRODUCTION

Poly(trimethylene terephthalate) (PTT) is a linear aromatic polyester being first synthesized by Whinfield and Dickson in 1941 [1], but it was not commercially available then due to the high production cost of 1,3-propanediol, one of its raw materials. PTT has recently been commercially made available by Shell Chemicals under the tradename Corterra®, thanks to a breakthrough in the synthesis of 1,3-propanediol at a much lower cost. PTT has properties intermediate to those of poly(ethylene terephthalate) (PET) and poly(buthylene terephthalate) (PBT), with an unusual combination of the outstanding properties of PET and processing characteristics of PBT. These characteristics make PTT highly suitable for uses in fibers, films, and engineering thermoplastics applications.

The extra number of methylene group in the repeating unit of PTT in comparison with that of PET is responsible for higher molecular flexibility for PTT molecules, resulting in PTT being more crystallizable than PET. The glass transition and the apparent melting temperatures for PTT were reported by Huang and Chang [2] to be ca. 44 and 228°C, respectively. Similar to PET and PBT, PTT crystallizes into triclinic crystal structure, with the periodicity along the *c*-axis containing two repeating units and the methylene groups being arranged in a highly contracted gauche-gauche conformation [3].

Recently, Chuah [4] studied the overall crystallization kinetics for PTT based on the Avrami model. He found that, for a given degree of undercooling, the crystallization rate for PTT lies between those for PET and PBT. He reported that PBT has the highest crystallization rates with the composite Avrami rate constant k_a being in the order of 10^{-2} to 10^{-1} min^{-n}, which is approximately an order of magnitude greater than PTT at 10^{-3} to 10^{-2} min^{-n}, which, in turn, is about an order of magnitude faster than PET at 10^{-4} to 10^{-2} min^{-n}. Similar results were also reported by Huang and Chang [2].

It is well established that nucleation mechanism plays an important role in crystallization of semi-crystalline polymers. Nucleation mechanisms can be categorized into two main processes: primary and secondary nucleation (i.e. subsequent crystal growth). Primary nucleation concerns with origination of the crystalline phase from a polymer solution or melt. It can be further categorized into

two types depending on the physical origins of the nucleus: homogeneous or heterogeneous. Secondary nucleation concerns with surface nucleation on an existing growth face, which is responsible for further growth of the activated nuclei.

In actual polymer processing, nucleation behavior (both primary and secondary) of a semi-crystalline polymer is characterized and controlled mainly by not only the presence of infusible heterogeneous nuclei (e.g., catalyst residues, nucleating agents, impurities, etc.), but the processing histories (e.g., temperature, pressure, shear stress, etc.) as well. Therefore, it is necessary that the nucleation mechanism and rate are better understood. Apart from the infusible heterogeneous nuclei, residual crystallites, which are clusters of molecules that retain their crystallographic arrangement of crystals as a result of insufficient or partial melting conditions, can act as predetermined athermal nuclei upon subsequent cooling. Such a phenomenon is known as 'self-nucleation' or 'crystalline memory' effect. Apart from thermal treatments, mechanical manipulations also occur in actual processing. Such mechanical deformational histories can lead to preferred orientation of polymer molecules which, in itself, can enhance nucleation rate. This effect is referred to as 'orientational memory' effect.

Both types of memory effects (i.e., crystalline and orientational) can affect a great deal to the crystallization behavior during subsequent cooling of a polymer part. To eliminate both kinds of memory effects, it is necessary to keep the part at a sufficiently high melt-annealing temperature T_f for a sufficiently long period of time (depending on the T_f used) in order to eradicate as many traces of crystalline and oriented aggregates as possible (i.e., complete melting). Practically, the T_f value for attaining complete melting is chosen such that it is greater than the equilibrium melting temperature T_m° of the polymer (i.e., $T_f > T_m^\circ$). In other cases, we wish to use these memory effects to preferably control the overall crystallization rate or morphology of the crystallizing polymer. Thus, we need to understand the characteristics of these effects in detail. Due to their importance, memory effects (i.e., either in the context of the crystalline or orientational memory effect, or both) have been of considerable interest and have been studied by several investigators [5-11].

In this present contribution, we focused on the effect of prior melt-annealing temperature T_f on the subsequent isothermal crystallization kinetics, crystalline structure, and subsequent melting behavior of neat and sheared PTT samples using differential scanning calorimetry (DSC) and wide-angle X-ray diffraction (WAXD) techniques. Even though the effect of T_f on the crystallization kinetics of polymers and the interpretation of such an effect based on the concept of self-nucleation have been well-documented (see, for example, references [5-11]), to our best knowledge that there have not been prior studies on PTT in the similar aspects.

2. THEORETICAL BACKGROUND

Isothermal bulk crystallization kinetics of semicrystalline polymers is commonly analyzed from the DSC crystallization exotherms [12-13] based primarily on the assumption that the evolution of crystallinity is linearly proportional to the evolution of heat released during the course of crystallization. Based on this notion, the relative crystallinity function of time $\theta(t)$ can be obtained according to the following equation:

$$\theta(t) = \frac{\int_0^t \left(\frac{dH_c}{dt}\right) dt}{\int_0^\infty \left(\frac{dH_c}{dt}\right) dt} \in [0,1] \qquad (1)$$

where t and $t = \infty$ are the elapsed time during the course of crystallization and at the end of crystallization process, respectively, and dH_c is the enthalpy of crystallization released during an infinitesimal time interval dt.

In order to quantitatively describe the macroscopic evolution of crystallinity during primary crystallization under quiescent isothermal conditions, a number of macrokinetics models have been proposed over the past sixty years: they are, for examples, the so-called 'Avrami' [14-19], Tobin [20-22], Malkin [23], and Urbanovici-Segal [24] macrokinetic models. In a previous work [25], qualitative comparison among the four macrokinetics models in describing isothermal crystallization data of PTT was carried out. The results suggested that the data were best described by the Urbanovici–Segal model, followed by the Avrami, Malkin, and Tobin models, respectively. Since the kinetics information obtained from both

Avrami and Urbanovici–Segal models is related and is comparatively of great interest, the isothermal crystallization data obtained in this work were analyzed according to these two models.

In the Avrami model [14-19], the relative crystallinity function of time $\theta(t)$ is related to the crystallization time t according to the equation:

$$\theta(t) = 1 - \exp\left[-(K_a t)^{n_a}\right] \in [0,1] \qquad (2)$$

where K_a and n_a are the Avrami crystallization rate constant and the Avrami exponent, respectively. Usually, the Avrami rate constant K_a is written in the form of the composite Avrami rate constant k_a (i.e. $k_a = K_a^n$). Since the units of k_a are a function of n_a, use K_a should be more preferable [26], since its units are given as an inverse of time. It should be noted that both K_a and n_a are constants specific to a given crystalline morphology and type of nucleation for a particular crystallization condition [27] and that, based on the original asssumptions of the theory, the value of the Avrami exponent n_a should be an integer ranging from 1 to 4.

Recently, Urbanovici and Segal [24] proposed a new kinetic equation, which is essentially a generalization of the Avrami model, the relation between the relative crystallinity function of time $\theta(t)$ and the crystallization time t is written as

$$\theta(t) = 1 - \left[1 + (r-1)(K_{us} t)^{n_{us}}\right]^{1/(1-r)} \in [0,1] \qquad (3)$$

where K_{us} and n_{us} are the Urbanovici–Segal crystallization rate constant and the Urbanovici–Segal exponent, respectively. The parameter r satisfies the condition $r > 0$. At the conditions where $r \to 1$, the Urbanovici–Segal model becomes identical to the Avrami model [24]. This simply means that parameter r is merely the factor determining the degree of deviation of the Urbanovici–Segal model from the Avrami model. It is also worth noting that both K_{us} and n_{us} have similar physical meanings to the Avrami kinetic parameters (i.e. K_a and n_a), and the units of K_{us} are given as an inverse of time.

3. EXPERIMENTAL

3.1. Material

Poly(trimethylene terephthalate) (PTT) was supplied in pellet form by Shell Chemicals (USA) (Corterra CP509201). The weight- and number-average molecular weights of this resin were determined to be ca. 78,100 and 34,700 Daltons, respectively. Molecular weight characterization for the PTT resin was carried out by Dr. Hoe H. Chuah and his co-workers of Shell Chemicals (USA) based on size-exclusion chromatography (SEC) technique.

3.2. Sample Preparation

Two types of samples, neat and sheared, were prepared. For neat samples, PTT pellets were first dried in a vacuum oven at 140°C for 5 hours. A film of ca. 200 μm in thickness was melt-pressed at 260°C using a Wabash V50H compression press under a clamping force of 10 tons. After 5 min, the film was taken out and allowed to cool at the ambient condition down to room temperature between the mold plates. For sheared samples, an Instron 4303 capillary rheometer (the L/D ratio and the diameter of the capillary were 40.16 and 1.25 mm, respectively) was used to prepare the samples at two different shear histories. Dried PTT pellets were first filled in the chamber, the temperature of which was set at 250°C, preheated for 10 min, and then extruded out at the wall shear rates of 92.1 and 245.6 s^{-1}. The extrudates were quenched in liquid nitrogen, in order to freeze the orientational state of the molecules and to prevent further changes from occurring. For simplicity, the as-prepared neat samples were hereafter called S0, while the as-prepared sheared samples using the wall shear rates of 92.1 and 245.6 s^{-1} were hereafter called S92.1 and S245.6, respectively.

3.3. Differential Scanning Calorimetry Measurements

A Perkin-Elmer Series 7 DSC was used to follow isothermal crystallization and subsequent melting behavior for these samples. Calibration for temperature scale was carried out using a pure indium standard (T_m° = 156.6 °C and ΔH_f° = 28.5 $J \cdot g^{-1}$) on every other run to ensure accuracy and reliability of the data obtained. To minimize thermal lag between polymer sample and DSC furnace, each sample holder was loaded with a sample weighing around 8.0 ± 0.3 mg, which was cut from the as-

prepared neat and sheared samples. It is worth noting that each sample was used only once and all the runs were carried out under nitrogen atmosphere to prevent extensive thermal degradation.

Each measurement started with heating a sample from 40°C at a heating rate of 80°C·min^{-1} to a desired melt-annealing temperature T_f, ranging from 260 to 300°C, for a fixed melt-annealing period t_h of 5 min. The sample was then rapidly cooled (i.e., at a cooling rate of ca. 200°C·min^{-1}) from the chosen T_f to a fixed crystallization temperature T_c of 200°C, where it was held until the crystallization process was considered complete (when no significant change in the heat flow as a function of time was further observed). The sample was then reheated again at a heating rate of 20°C·min^{-1} in order to observe the subsequent melting behavior. The analysis was carried out by directly fitting the experimental, isothermal crystallization data to the aforementioned macrokinetic models using a non-linear multivariable regression program.

3.4. Crystal Structure and Crystallinity Measurements

Wide-angle X-ray diffraction (WAXD) technique was used to determine the crystal modification and the apparent degree of crystallinity for neat PTT samples, which had been prepared in DSC according to the isothermal crystallization condition set forth for the DSC measurements (viz. after complete crystallization at a T_c of 200°C, the samples were then cooled at a cooling rate of ca. 200°C·min^{-1} to 30°C without a subsequent heating scan). Each sample was then taken out of a DSC sample holder and was pasted onto a glass sample holder. The WAXD intensity patterns for each sample was recorded on a Rigaku Rint 2000 diffractometer, equipped with a computerized data collection and analytical tools. The X-ray source (CuKα radiation, λ = 1.54 Å) was operated at an applied voltage of 40 kV and a filament current of 30 mA.

4. RESULTS AND DISCUSSION

4.1. Subsequent Isothermal Crystallization Behavior

Figures 1 to 3 illustrate subsequent isothermal crystallization exotherms for S0, S92.1, and S245.6 samples isothermally crystallized at a fixed crystallization

temperature T_c of 200°C after being partially or completely melted at different melt-annealing temperatures T_f, ranging from 260 to 300°C, for a fixed melt-annealing period t_h of 5 min. The results shown in these figures clearly suggest that even though the samples were isothermally crystallized at the same temperature, choices of the T_f used to melt the samples played an important role in determining their subsequent crystallization behavior. According to these figures, it is qualitatively obvious that, at low T_f's, the crystallization proceeded very rapidly with low values of the induction period T_i, and that the positions of the peak temperature for these exotherms was found to increase with increasing T_f used up to a certain critical T_f value, after which point the position of the peak temperature appeared to be unaffected by changes in the T_f used.

Further analysis of the experimental data can be carried out by converting the raw experimental data such as those shown in Figures 1 to 3 to the relative crystallinity functions of time $\theta(t)$. Figure 4 shows, for examples, the typical relative crystallinity function of time $\theta(t)$ (after subtraction of the induction period T_i) for S0 samples isothermally crystallized at 200°C after being partially or completely melted at different T_f's, ranging from 260 to 275°C, for 5 min (the raw data are shown as different geometrical points). Figure 4 illustrates the effect of the T_f used on the resulting subsequent isothermal crystallization behavior. For a given sample type, the time to reach the ultimate crystallinity (i.e., complete crystallization) increased with increasing T_f used up to a certain critical T_f value and then it was leveled off afterwards.

The effect of shear on subsequent isothermal crystallization behavior of PTT is illustrated in Figure 5, where the relative crystallization function of time $\theta(t)$ (after subtraction of the induction period T_i) for S0, S92.1, and S245.6 samples isothermally crystallized at 200°C after being partially or completely melted at T_f of 270°C for 5 min is shown. Clearly, the times to complete the crystallization process for both sheared samples was much greater than that for neat sample. In addition, the induction period T_i for neat sample was found to be much greater than those for sheared samples, with the values being ca. 1.1, 0.5, and 0.4 min for S0, S92.1, and S245.6 samples, respectively. An increase in both the primary nucleation and the

bulk crystallization rates may be a result of the lowered activation energy for formation and the increased number of the primary nuclei, respectively.

Figure 6 illustrates plots of half-time of crystallization $t_{0.5}$, which is defined as the elapsed crystallization time from the onset to 50% completion and can be directly determined from the experimental $\theta(t)$ functions, as a function of T_f, ranging from 260 to 300°C, for all of the samples studied. For S0 samples, it is apparent that the $t_{0.5}$ values and the bulk crystallization rate (presented in Figure 7 in the form of the reciprocal values of the half-time of crystallization, i.e., $t_{0.5}^{-1}$) exhibited strong correlations with the T_f used within the range $T_f \leq$ ca. 275°C, while they became less dependent of T_f within the range $T_f \geq$ ca. 275°C. For S92.1 and S245.6 samples, both the observed $t_{0.5}$ and the resulting $t_{0.5}^{-1}$ values exhibited strong correlations with the T_f used within the range $T_f \leq$ ca. 280°C, while they became less dependent of T_f within the range $T_f \geq$ ca. 280°C. It should be noted that the resulting $t_{0.5}^{-1}$ values for all of the samples studied are summarized in Table 1.

Within the range $T_f \leq 275$°C for S0 samples and $T_f \leq 280$°C for S92.1 and S245.6 samples, the observed $t_{0.5}$ values were found to increase monotonically, while the resulting $t_{0.5}^{-1}$ values decreased, with increasing T_f. Within the range $T_f \geq 275$°C for S0 samples and $T_f \geq 280$°C for S92.1 and S245.6 samples, the observed $t_{0.5}$ values were found to decrease slightly, while the resulting $t_{0.5}^{-1}$ values increased very slightly, with increasing T_f. In syndiotactic polypropylene (s-PP) [11], it was found that the observed $t_{0.5}$ values for all of the s-PP resins studied did not change with increasing T_f when T_f was greater than the critical T_f value (i.e., 160°C for all of the resins studied). The slight decrease and the slight increase in the $t_{0.5}$ and the $t_{0.5}^{-1}$ values, respectively, for all of the samples studied with increasing T_f when T_f was greater than the respective critical T_f values (i.e., $(T_f^{cr})_{S0} \approx 275$°C and $(T_f^{cr})_{S92.1} = (T_f^{cr})_{S245.6} \approx 280$°C) are the phenomenon which is different from what had been observed in s-PP and the most likely explanation may be the reduction in the molecular weight averages of the PTT resin as a result of thermal degradation, especially at high T_f values (i.e., 300°C).

Comparatively among all of the sample types studied, it was found that, within the whole T_f range investigated, S245.6 samples crystallized the fastest,

followed by S92.1 and S0 samples, respectively. The results suggest that the bulk crystallization rates for PTT were greatly enhanced by the effect of shear. The increase in the bulk crystallization rates were most significant in samples melted at T_f's lower than the respective critical T_f values, in which a three-fold and two-fold increase in the bulk crystallization rates were observed for S245.6 and S92.1 samples over those for S0 samples. Very interesting and unlikely results were observed among all of the sample types studied, in that, within the range where T_f's were greater than the respective critical T_f values, S245.6 samples showed slightly higher bulk crystallization rates than S92.1 and S0 samples did, respectively. The most likely explanation may be a result of the effect of shear on the reduction in the molecular weight averages of the PTT resin. As a result, S245.6 samples which were sheared at the highest shear rate should show the most significant molecular weight reduction, hence the highest bulk crystallization rates, over the S92.1 and S0 samples, respectively.

4.2 Subsequent Isothermal Crystallization Kinetics

In order to observe the effect of prior melt-annealing temperature on the subsequent isothermal crystallization kinetics for both neat and sheared samples, the experimental $\theta(t)$ data collected on all of the samples studied were analyzed according to the Avrami and Urbanovici–Segal macrokinetic models (i.e., Equations (2) and (3), respectively).

4.2.1. Avrami Analysis

Data analysis based on the Avrami macrokinetic model was carried out by directly fitting the experimental $\theta(t)$ data to Equation (2) (shown, for examples, in Figure 4 as dashed lines) using the direct data-fitting procedure [28]. Table 1 summarizes values of the Avrami kinetic parameters (i.e., n_a and K_a) as well as the values of the correlation parameter r^2 as a result of the best fits. According to Table 1, the n_a values were found to range from ca. 2.0 to 2.8 for S0 samples, from ca. 1.7 to 2.9 for S92.1 samples, and from ca. 1.5 to 2.9 for S245.6 samples. Similar to the case of $t_{0.5}^{-1}$ (see Figure 7), values of K_a, shown in Figure 8, were found to be strongly affected by changes in the T_f used within the range $T_f \leq$ ca. 275°C for S0

samples and $T_f \leq$ ca. 280°C for S92.1 and S245.6 samples, while they became less dependent on T_f with a slight increase in the values with increasing T_f within the T_f range greater than the respective critical T_f values. The similarity between $t_{0.5}^{-1}$ and K_a is expected, since K_a relates to $t_{0.5}^{-1}$ according to the following equation:

$$K_a = (\ln 2)^{1/n_a} t_{0.5}^{-1} \quad (4)$$

The calculated values of K_a, summarized in Table 1 as K_a*, were found to be in good agreement with the experimental values, with the calculated value being 1.1% for S0 samples, 2.4% for S92.1 samples, and 0.8% for S245.6 samples different from the experimental values on average.

4.2.2. Urbanovici-Segal Analysis

Similar to the case of the Avrami analysis, data analysis based on the Urbanovici–Segal macrokinetic model was carried out by directly fitting the experimental $\theta(t)$ data to Equation (3) (shown, for examples, in Figure 4 as solid lines) using the direct data-fitting procedure [28]. Table 2 summarizes values of the Urbanovici-Segal kinetic parameters (i.e., n_{us}, K_{us}, and r) as well as the values of the correlation parameters r^2 as a result of the best fits. According to Table 2, the n_{us} values were found to range from ca. 2.1 to 3.1 for S0 samples, from ca. 2.0 to 3.0 for S92.1 samples, and from ca. 2.2 to 3.0 for S245.6 samples. Similar to the cases of $t_{0.5}^{-1}$ (see Figure 7) and K_a (see Figure 8), values of K_{us}, shown in Figure 9, were also found to be strongly dependent on changes in the T_f used within the range $T_f \leq$ ca. 275°C for S0 samples and $T_f \leq$ ca. 280°C for S92.1 and S245.6 samples, while they became less dependent on T_f with a slight increase in the values with increasing T_f within the T_f range greater than the respective critical T_f values. Again, the similarity between $t_{0.5}^{-1}$ and K_{us} is not surprising, since K_{us} can be calculated directly from $t_{0.5}^{-1}$ according to the following equation:

$$K_{us} = \left(\frac{0.5^{(1-r)} - 1}{r - 1} \right)^{1/n_{us}} t_{0.5}^{-1} \quad (5)$$

The calculated values of K_{us}, listed in Table 2 as K_{us}*, were found to be in good agreement with the experimental values, with the calculated values being 0.1% for

S0 samples, 1.9% for S92.1 samples, and 0.2% for S245.6 samples different from the experimental values on average.

Comparison between the kinetic parameters obtained from fitting the experimental data to the Avrami and Urbanovici–Segal models (see Tables 1 and 2) indicated that the extent of the discrepancies between the Urbanovici–Segal and Avrami kinetic parameters depended solely on the values of the parameter r obtained from the fits. It was earlier stated that the Urbanovici–Segal model becomes identical to the Avrami model when r approaches one [24]. By referring to Tables 1 and 2, it is evident that, when $r > 1$, the values of the Urbanovici–Segal kinetic parameters were systematically greater than those of the Avrami ones, and the greater value of r was from 1, the greater the values of the Urbanovici–Segal parameters were than those of the Avrami ones. On the contrary, when $r < 1$, the values of the Urbanovici–Segal parameters were systematically less than those of the Avrami ones, and as the lesser the value of r was from 1, the lesser the values of the Urbanovici–Segal kinetic parameters were than those of the Avrami ones.

4.3. Crystal Modification and Apparent Degree of Crystallinity

The objectives for the WAXD experiment were two-fold: (1) to investigate whether or not the partial or complete melting conditions affect the formation of crystals during crystallization, and (2) to investigate whether or not the partial or complete melting conditions affect the amount of the crystalline content formed. Figure 10 illustrates, for examples, the WAXD patterns for S0 samples isothermally crystallized at 200°C after partially or completely melted at different T_f's, ranging from 260 to 300°C, for 5 min. It should be noted that the measurements were carried out only on neat PTT samples (i.e., S0 samples). However, in sheared samples, WAXD was used to verify that crystallization did not occur during quenching.

According to Figure 10, all of the diffractograms exhibited major characteristic crystalline peaks at the scattering angles 2θ of ca. 15.4 ± 0.1, 19.4 ± 0.1, 21.8 ± 0.1, 23.6 ± 0.1, 24.8 ± 0.1, and 27.7 ± 0.1, respectively. According to related published work on crystallographical studies of PTT [29,30], the crystalline structure of these samples deduced from the diffractograms shown in Figure 10 can

be designated as a triclinic unit cell with the unit cell parameters being a = 4.64 Å, b = 6.27 Å, and c = 18.64 Å, α = 98°, β = 90°, and γ = 111°, which exhibits an anti-chiral packing of chains only along the c-axis, and the space group proposed for this crystal modification was $P\bar{1}$ [29]. According to this space group, the major characteristic WAXD peaks should be observed at the scattering angles 2θ of ca. 15.3, 16.8, 19.4, 21.8, 23.6, 24.6 and 27.3°, corresponding to the reflection planes of (010), $(0\bar{1}2)$, (012), $(10\bar{2})$, (102), $(1\bar{1}3)$, and $(10\bar{4})$, respectively [31].

One simple method used to estimate the apparent degree of crystallinity from a one-dimensional powder WAXD pattern is to compute the integrated intensities of the pattern associated with the crystalline structure and the amorphous halo. To a first approximation, the apparent degree of crystallinity is obtained based on an assumption that the total scattering within a certain region of reciprocal space is independent of the state of morphological aggregation of the materials [32]. The apparent degree of crystallinity χ_c^{WAXD} can then be expressed by the mass fraction of crystalline aggregates, and can be determined from the ratio of the integrated WAXD intensities under the crystalline peaks A_c to the integrated total WAXD intensities A_t (i.e., $A_t = A_c + A_a$, where A_a is the integrated WAXD intensities under the amorphous halo). According to this procedure, the χ_c^{WAXD} values obtained from the WAXD patterns shown in Figure 10 were 26.4, 28.7, 30.5, 33.3, and 35.6% for S0 samples melted at T_f values of 260, 270, 280, 290, and 300°C, respectively, for 5 min before isothermally crystallized at 200°C. The reason for an increase in the χ_c^{WAXD} value with increasing T_f is not certain at this point, but it is thought to be the effect of the reduced molecular weight averages due to thermal degradation, which was responsible for increased bulk crystallization rates observed.

4.4. Subsequent Melting Behavior

Figures 11 to 13 illustrate subsequent melting endotherms for S0, S92.1, and S245.6 samples isothermally crystallized at 200°C after being partially or completely melted at various T_f's, ranging from 265 to 300°C, for 5 min. Two major melting endotherms were clearly visible on all of the endotherms shown. Based on our earlier results on multiple melting behavior in isothermally crystallized PTT [33],

these two endotherms were designated as the low- and the middle-temperature melting endotherms, of which peak temperatures were denoted as the low-melting peak temperature T_I and the middle-melting peak temperature T_{II}, respectively. The occurrence of peak I was a result of the melting of the primary crystals formed at the T_c and peak II was a result of the melting of the recrystallized crystals formed during a heating scan [33].

Qualitatively, the peak positions of the two endotherms for each sample type were not much affected by choices of the T_f used to melt the samples (see Figures 11 to 13). Quantitatively, the average values of T_I and T_{II}, for S0 samples, were ca. 218.5 and 227.8°C, respectively; for S92.1 samples, were ca. 218.9 and 228.5°C, respectively; and, for S245.6 samples, were 219.2 and 229.2°C, respectively. The results obtained suggest that both neat and sheared samples showed similar subsequent melting behavior, in spite of the fact that the bulk crystallization rates (i.e., $t_{0.5}^{-1}$, K_a, and K_{us}) suggested a strong dependence on choices of the T_f used to melt the sample, when T_f was lower than the respective critical T_f values. The almost-identical T_I values observed for different sample types further imply that the lamellar thickness was not affected by shear, but was only dictated by choices of the T_c used to crystallize the samples.

5. CONCLUSIONS

In this present contribution, the effect of prior melt-annealing temperature T_f on the subsequent isothermal crystallization kinetics, crystalline structure, and subsequent melting behavior of neat and sheared poly(trimethylene terephthalate) (PTT) samples were investigated using differential scanning calorimetry (DSC) and wide-angle X-ray diffraction (WAXD) techniques in order to illustrate the effects of crystalline and orientational memory phenomena on subsequent isothermal crystallization and subsequent melting behavior of PTT. On partial melting, the DSC experiment suggested that the choice of the T_f used to melt the samples played an important role in determining their bulk crystallization rates, in which the bulk crystallization rate parameters studied (i.e., $t_{0.5}^{-1}$, K_a, and K_{us}) were all found to decrease monotonically with increasing T_f. The decrease in the values of these rate parameters with T_f continued up to a critical T_f value (i.e., ca. 275°C for neat PTT

samples and ca. 280°C for PTT samples which were sheared with shear rates of 92.1 and 245.6 s^{-1}). At this point, the values of the rate parameters reached a minimum and then slightly increased afterwards. The slight increase in the values of the rate parameters after a critical T_f value was postulated as a result of the reduction in the molecular weight averages of the samples due to thermal degradation, which caused the bulk crystallization rates to slightly increase. The WAXD results suggested that neat PTT samples which were subject to different T_f's crystallized into the same triclinic unit cell; however, the apparent degree of crystallinity was found to slightly increase with increasing T_f used to melt the samples. Lastly, the subsequent melting behavior suggested that the T_f used to melt the samples had no effect on the peak positions of both low- and middle-temperature melting endotherms observed and that the observed peak values of these endotherms for all of the neat and sheared samples studied were almost identical.

6. ACKNOWLEDGMENTS

The authors wish to thank Dr. Hoe H. Chuah of Shell Chemicals (USA) for supply and for carrying out the molecular weight measurement of the PTT resin used. PS acknowledges a grant provided by Chulalongkorn University through the Development Grants for New Faculty/Researchers. Partial support from the Petroleum and Petrochemical Technology Consortium and the Petroleum and Petrochemical College is greatly acknowledged.

REFERENCES

[1] Whinfield JR and Dickson JT, Brit Pat 578,079 (June 14, 1946).

[2] Huang JM and Chang FC, J Polym Sci – Polym Phys 2000, 38, 934.

[3] Chuah H, in Scheirs J and Long T ed. "Modern Polyester," John Wiley & Sons, New York, 2003, Chapter 11.

[4] Chuah H, Polym Engng Sci 2001, 41, 308.

[5] Wunderlich B, in "Macromolecular physics," vol. 2., New York, Academic Press, 1976, pp 52-70.

[6] Khanna YP, Kumar R, and Reimschuessel AC, Polym Engng Sci 1988, 28, 1612.

[7] Mehl NA and Rebenfeld L, Polym Engng Sci 1992, 32, 1451.

[8] Ziabicki A and Alfonso GC, Colloid Polym Sci 1994, 272, 1027.

[9] Alfonso GC and Scardigli P, Macromol Symp 1997, 118, 323.

[10] Feng Y and Jin X, J Appl Polym Sci 1999, 72, 1559.

[11] Supaphol P and Lin JS, Polymer 2001, 42, 9617.

[12] Hay JN and Sabir M, Polymer 1969, 10, 203.

[13] Hay JN, Brit Polym J 1979, 11, 137.

[14] Kolmogorov AN, Izvestiya Akad USSR – Ser Math 1937, 1, 355.

[15] Johnson WA and Mehl KF, Trans Am Inst Mining Met Eng 1939, 135, 416.

[16] Avrami M, J Chem Phys 1939, 7, 1103.

[17] Avrami M, J Chem Phys 1940, 8, 212.

[18] Avrami M, J Chem Phys 1941, 9, 177.

[19] Evans UR, Trans Faraday Soc 1945, 41, 365.

[20] Tobin MC, J Polym Sci – Polym Phys 1974, 12, 399.

[21] Tobin MC, J Polym Sci – Polym Phys 1976, 14, 2253.

[22] Tobin MC, J Polym Sci – Polym Phys 1977, 15, 2269.

[23] Malkin AY, Beghishev VP, Keapin IA, and Bolgov SA, Poym Engng Sci 1984, 24, 1396.

[24] Urbanovici E and Segal E, Thermochim Acta 1990, 171, 87.

[25] Dangseeyun N, Srimoaon P, Supaphol P, and Nithitanakul M, Thermochim Acta, submitted.

[26] Supaphol P, Thermochim Acta 2001, 370, 37.

[27] Wunderlich B, in "Macromolecular Physics," Vol. 2, Academic Press, New York, 1976, p 132.

[28] Supaphol P and Spruiell JE, J Macromol Sci – Phys 2000, 39, 257.

[29] Desborough IJ, Hall IH, and Neisser JZ, Polymer 1979, 20, 419.

[30] Dandurand SP, Perez S, Revol JF, and Brisse F, Polymer 1979, 20, 419.

[31] Wang B, Li YC, Hanzlicek J, Cheng SZD, Gail PH, Grebowicz J, and Ho RM, Polymer 2001, 42, 7171.

[32] De Rosa C, Auriemma F, and Vinti V, Macromolecules 1997, 30, 4137.

[33] Srimoaon P, Dangseeyun N, and Supaphol P, Eur Polym J, submitted.

CAPTIONS OF FIGURES

Figure 1 Subsequent isothermal crystallization exotherm for neat PTT samples isothermally crystallized at 200°C after being melted at each respective melt-annealing temperature T_f for 5 min.

Figure 2 Subsequent isothermal crystallization exotherm for sheared PTT samples (at 92.1 s^{-1}) isothermally crystallized at 200°C after being melted at each respective melt- annealing temperature T_f for 5 min.

Figure 3 Subsequent isothermal crystallization exotherm for sheared PTT samples (at 245.6 s^{-1}) samples isothermally crystallized at 200°C after being melted at each respective melt-annealing temperature T_f for 5 min.

Figure 4 Typical relative crystallinity function of time $\theta(t)$ for neat PTT samples isothermally crystallized at 200°C after being melted at each respective melt-annealing temperature T_f for 5 min. The raw data, shown as various geometrical points, were fitted to the Avrami and Urbanovici–Segal macrokinetic models, with the beat fits being shown as dashed and solid lines, respectively.

Figure 5 Relative crystallinity function of time $\theta(t)$ for all of the neat and sheared samples studied, which were isothermally crystallized at 200°C after being melted at a melt-annealing temperature T_f of 270°C for 5 min.

Figure 6 Variation of the crystallization half-time $t_{0.5}$ as a function of the melt-annealing temperature T_f for all of the neat and sheared PTT samples studied.

Figure 7 Variation of the reciprocal value of the crystallization half-time $t_{0.5}^{-1}$ as a function of the melt-annealing temperature T_f for all of the neat and sheared PTT samples studied.

Figure 8 Variation of the Avrami rate constant K_a as a function of the melt-annealing temperature T_f for all of the neat and sheared PTT samples studied.

Figure 9 Variation of the Urbanovici–Segal rate constant K_{us} as a function of the

Table 1 Overall crystallization kinetic data for all of the PTT samples studied based on the Avrami analysis

	S0					S92.1					S245.6				
T_c °C	$t_{0.5}^{-1}$ min^{-1}	n_a	K_a min^{-1}	r^2	K_a^* min^{-1}	$t_{0.5}^{-1}$ min^{-1}	n_a	K_a min^{-1}	r^2	K_a^* min^{-1}	$t_{0.5}^{-1}$ min^{-1}	n_a	K_a min^{-1}	r^2	K_a^* min^{-1}
260	0.417	1.86	0.335	0.997	0.342	0.741	1.65	0.581	0.9989	0.594	1.236	1.50	0.953	0.9948	0.968
265	0.227	2.06	0.186	0.998	0.190	0.646	1.84	0.526	0.9998	0.530	1.095	1.86	0.891	0.9995	0.899
270	0.152	2.69	0.133	1.000	0.132	0.479	1.86	0.389	0.9995	0.394	0.712	2.07	0.591	0.9997	0.596
273	-	-	-	-	-	0.227	2.16	0.175	0.9998	0.192	0.309	2.33	0.263	0.9999	0.264
275	0.119	2.52	0.103	1.000	0.103	0.209	2.44	0.139	0.9996	0.180	0.228	2.65	0.198	1.0000	0.198
278	-	-	-	-	-	0.170	2.47	0.147	0.9998	0.146	0.181	2.64	0.160	0.9997	0.158
280	0.122	2.70	0.104	0.999	0.106	0.153	2.46	0.132	0.9997	0.131	0.163	2.76	0.142	0.9998	0.143
282	0.127	2.82	0.110	0.999	0.111	0.152	2.81	0.133	1.0000	0.133	-	-	-	-	-
285	0.129	2.27	0.109	1.000	0.110	0.152	2.70	0.133	0.9999	0.133	0.167	2.45	0.145	0.9997	0.144
290	0.137	2.65	0.120	1.000	0.119	0.164	2.88	0.148	0.9999	0.144	0.170	2.88	0.148	0.9998	0.150
300	0.163	1.96	0.135	1.000	0.136	0.186	2.63	0.170	0.9998	0.161	0.195	2.63	0.170	0.9998	0.170

Table 2 Overall crystallization kinetic data for all of the PTT samples studied based on the Urbanovici-Segal analysis

	S0						S92.1						S245.6					
T_f °C	$t_{0.5}^{-1}$ min^{-1}	n_{us}	K_{us} min^{-1}	r	r^2	K_{us}^* min^{-1}	$t_{0.5}^{-1}$ min^{-1}	n_{us}	K_{us} min^{-1}	r	r^2	K_{us}^* min^{-1}	$t_{0.5}^{-1}$ min^{-1}	n_{us}	K_{us} min^{-1}	r	r^2	K_{us}^* min^{-1}
260	0.417	2.59	0.402	1.712	0.9998	0.400	0.741	1.99	0.647	1.330	0.9996	0.654	1.236	2.53	1.225	1.940	0.9996	1.225
265	0.227	2.61	0.211	1.500	0.9998	0.211	0.646	2.01	0.554	1.170	0.9999	0.555	1.095	2.18	0.971	1.300	1.0000	0.972
270	0.152	2.50	0.128	0.835	0.9999	0.128	0.479	2.15	0.420	1.260	0.9999	0.422	0.712	2.31	0.625	1.210	1.0000	0.627
273	-	-	-	-	-	-	0.227	2.35	0.183	1.170	0.9999	0.199	0.309	2.28	0.260	0.960	0.9999	0.262
275	0.119	2.66	0.105	1.100	0.9998	0.105	0.209	2.66	0.146	1.230	0.9999	0.188	0.228	2.60	0.197	0.960	1.0000	0.197
278	-	-	-	-	-	-	0.170	2.51	0.149	1.060	0.9999	0.148	0.181	2.42	0.152	0.820	1.0000	0.152
280	0.122	3.11	0.109	1.310	0.9996	0.112	0.153	2.59	0.136	1.160	0.9999	0.135	0.163	2.94	0.145	1.130	0.9999	0.146
282	0.127	2.76	0.108	0.963	0.9994	0.110	0.152	2.79	0.133	0.980	1.0000	0.133	-	-	-	-	-	-
285	0.129	2.35	0.112	1.100	0.9998	0.112	0.152	2.70	0.133	0.990	0.9999	0.133	0.167	2.46	0.145	1.010	0.9998	0.144
290	0.137	2.63	0.120	0.948	0.9995	0.118	0.164	2.98	0.150	1.070	1.0000	0.146	0.170	2.98	0.150	1.070	0.9980	0.152
300	0.163	2.12	0.141	1.153	0.9999	0.141	0.186	2.48	0.164	0.843	0.9999	0.157	0.195	2.48	0.164	0.840	1.0000	0.165

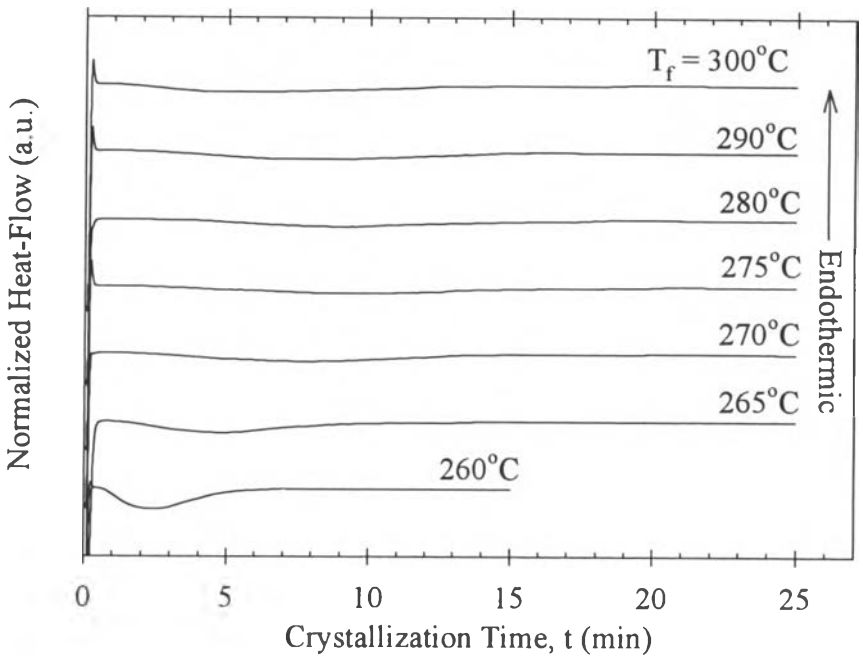
$T_f = 300°C$
290°C
280°C
275°C
270°C
265°C
260°C
Endothermic
Normalized Heat-Flow (a.u.)
0
5
10
15
20
25
Crystallization Time, t (min)

Figure 1

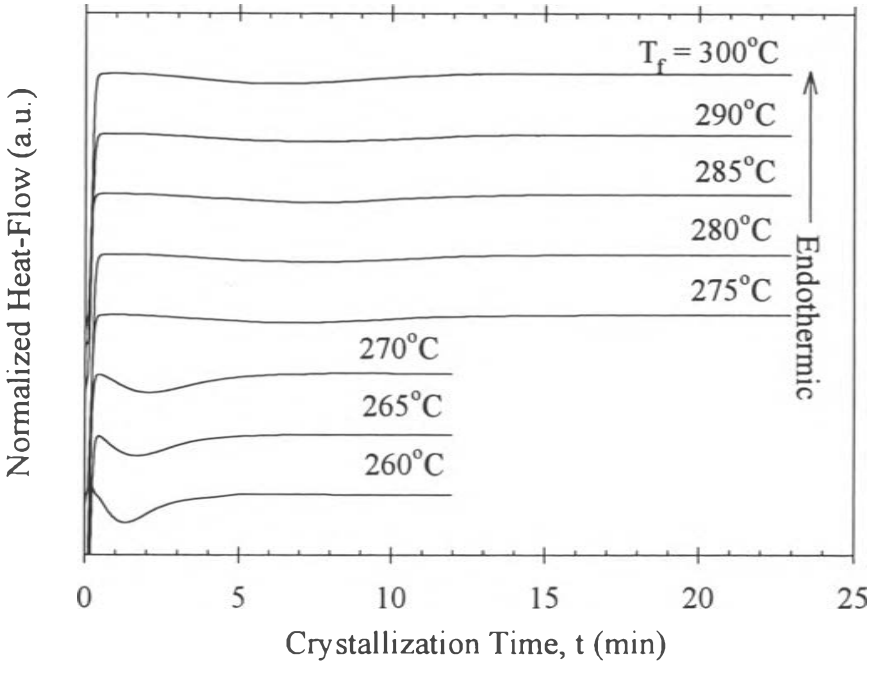
T_f = 300°C
290°C
285°C
280°C
275°C
270°C
265°C
260°C
Endothermic
Normalized Heat-Flow (a.u.)
0
5
10
15
20
25
Crystallization Time, t (min)

Figure 2

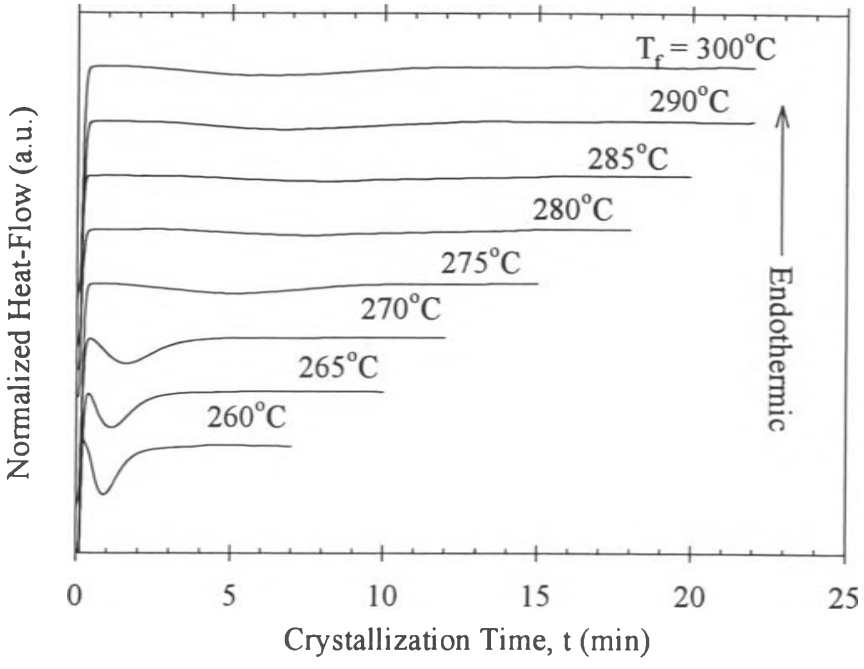
T_f = 300°C
290°C
285°C
280°C
275°C
270°C
265°C
260°C
Endothermic
Normalized Heat-Flow (a.u.)
0
5
10
15
20
25
Crystallization Time, t (min)

Figure 3

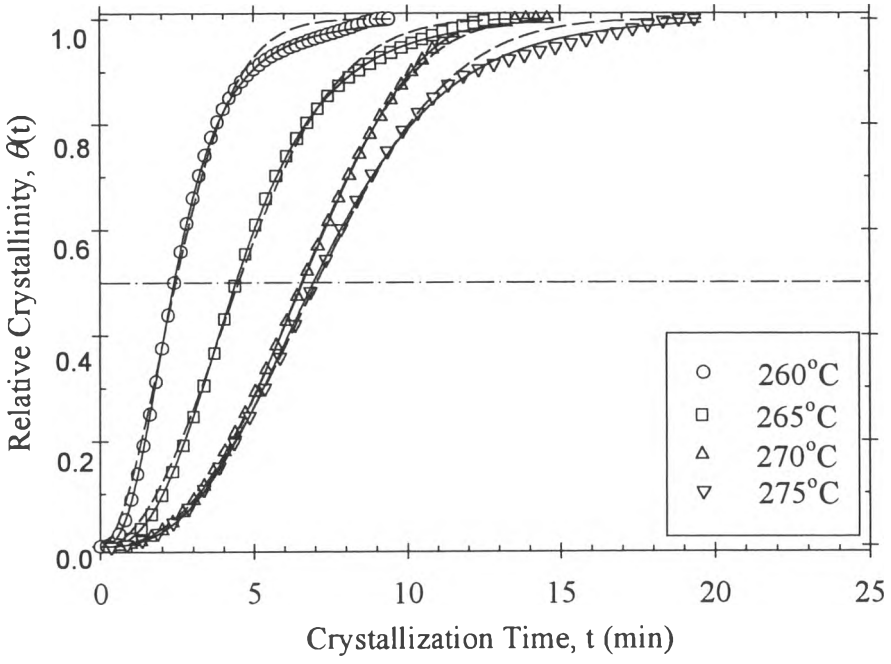
Relative Crystallinity, θ(t)
1.0
0.8
0.6
0.4
0.2
0.0
0
5
10
15
20
25
Crystallization Time, t (min)
260°C
265°C
270°C
275°C

Figure 4

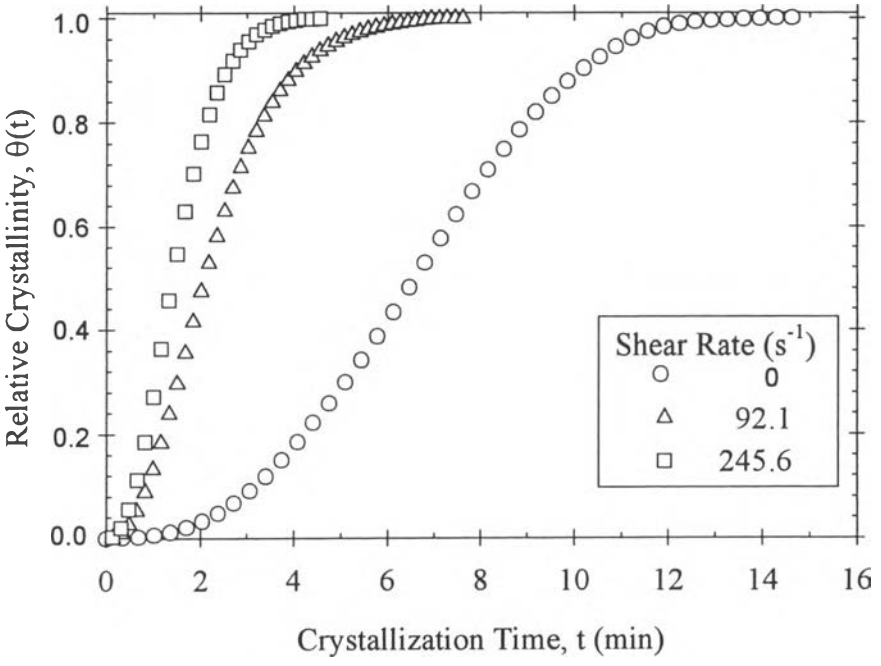
Relative Crystallinity, θ(t)
1.0
0.8
0.6
0.4
0.2
0.0
0
2
4
6
8
10
12
14
16
Crystallization Time, t (min)
Shear Rate (s-1)
0
92.1
245.6

Figure 5

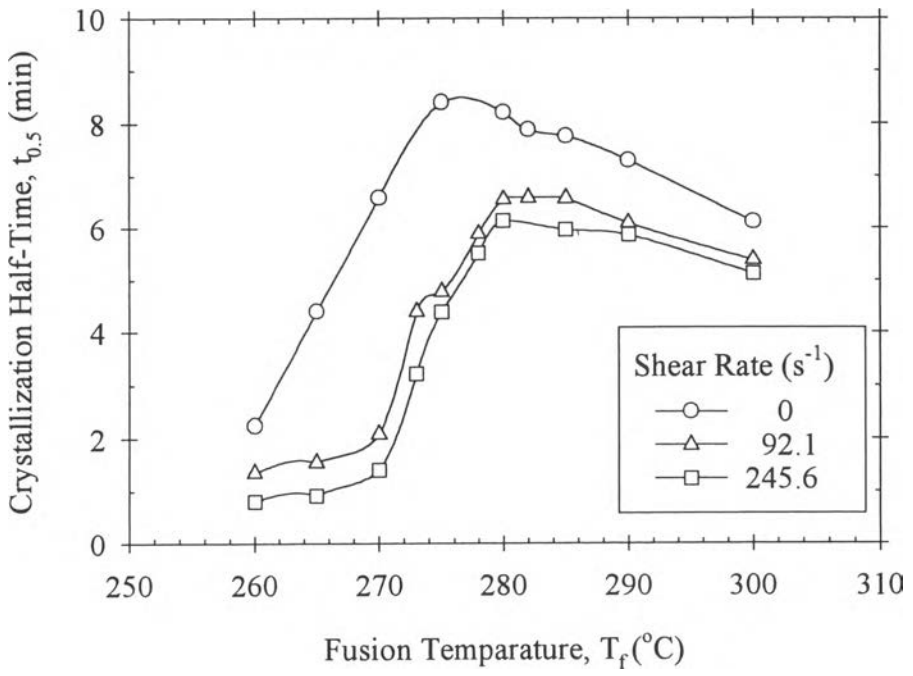
Crystallization Half-Time, $t_{0.5}$ (min)
10
8
6
4
2
0
250
260
270
280
290
300
310
Fusion Temparature, T_f(°C)
Shear Rate (s^{-1})
0
92.1
245.6

Figure 6

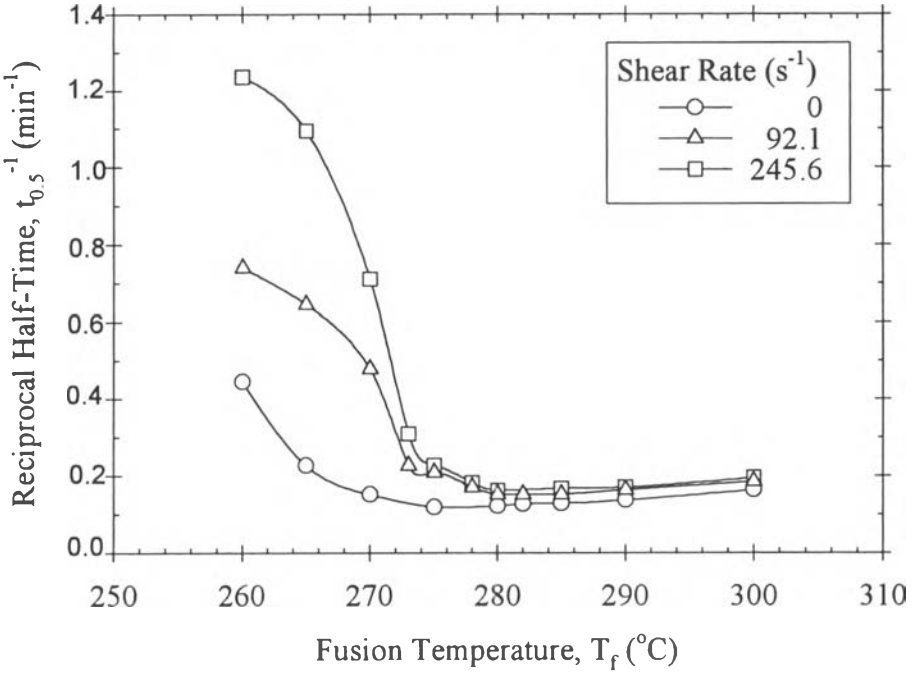
Shear Rate (s^{-1})
0
92.1
245.6
Reciprocal Half-Time, $t_{0.5}^{-1}$ (min^{-1})
Fusion Temperature, T_f (°C)
1.4
1.2
1.0
0.8
0.6
0.4
0.2
0.0
250
260
270
280
290
300
310

Figure 7

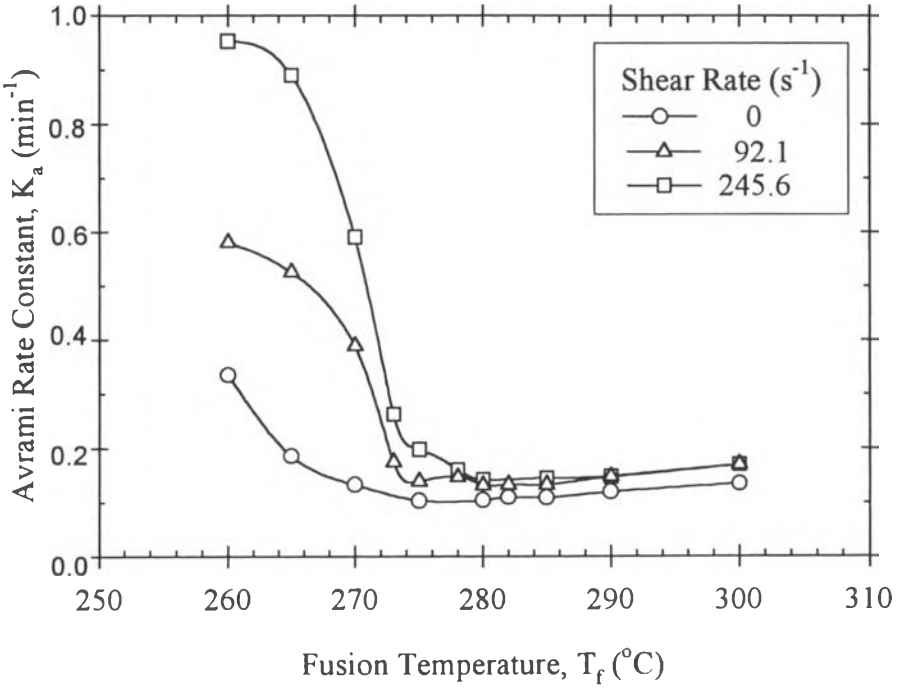
Shear Rate (s^{-1})
0
92.1
245.6
Avrami Rate Constant, K_a (min^{-1})
Fusion Temperature, T_f (°C)
1.0
0.8
0.6
0.4
0.2
0.0
250
260
270
280
290
300
310

Figure 8

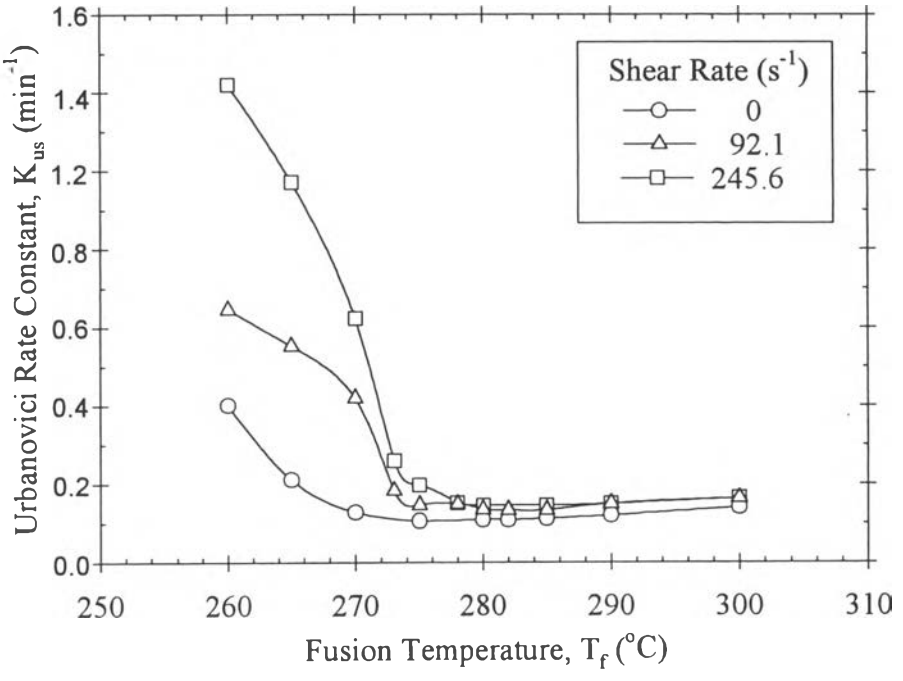
Urbanovici Rate Constant, K_{us} (min^{-1})
1.6
1.4
1.2
0.8
0.6
0.4
0.2
0.0
250
260
270
280
290
300
310
Fusion Temperature, T_f (°C)
Shear Rate (s^{-1})
0
92.1
245.6

Figure 9

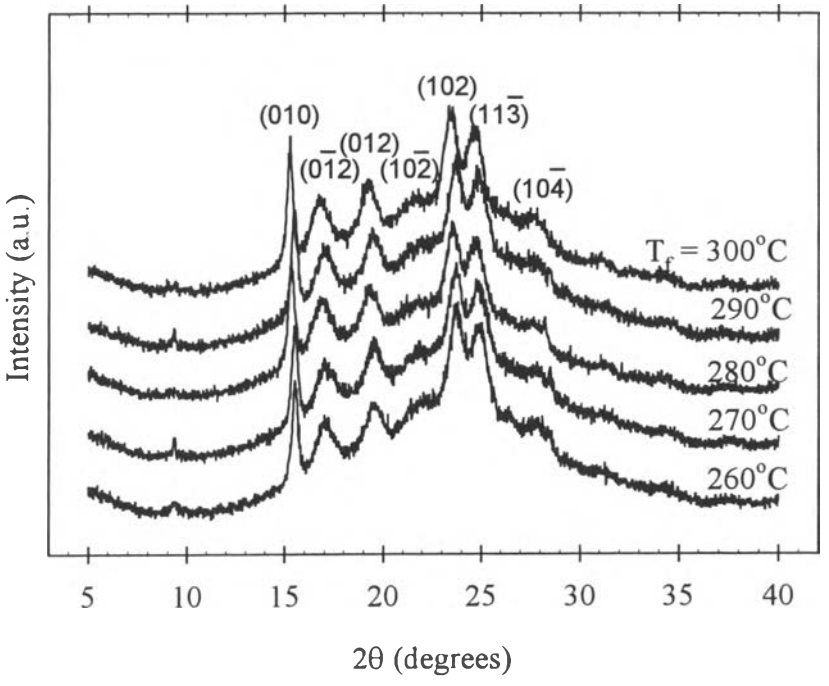
(010)
(012)
(012)
(102)
(102)
(113)
(104)
T_c = 300°C
290°C
280°C
270°C
260°C
Intensity (a.u.)
5
10
15
20
25
30
35
40
2θ (degrees)

Figure 10

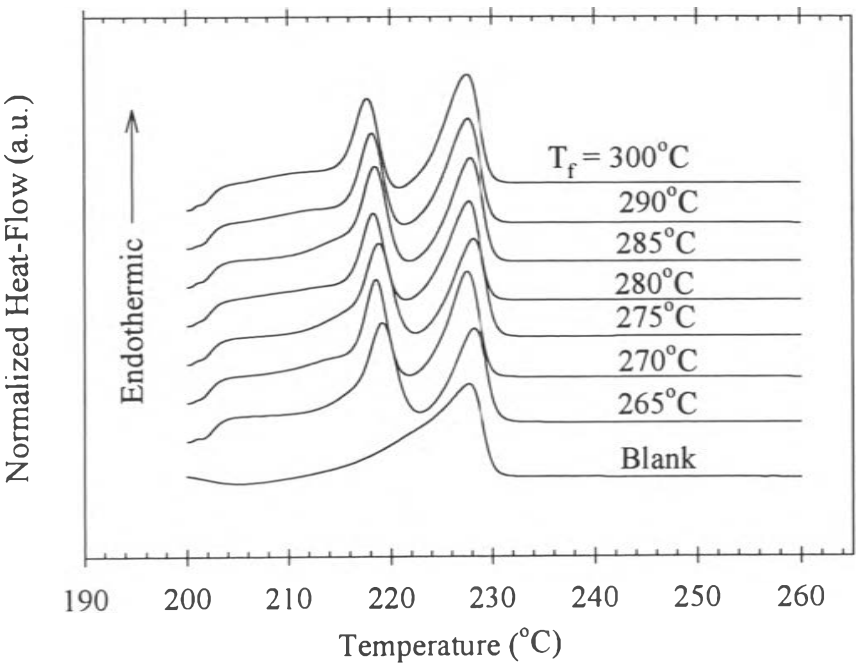
Normalized Heat-Flow (a.u.)
Endothermic
T_f = 300°C
290°C
285°C
280°C
275°C
270°C
265°C
Blank
190
200
210
220
230
240
250
260
Temperature (°C)

Figure 11

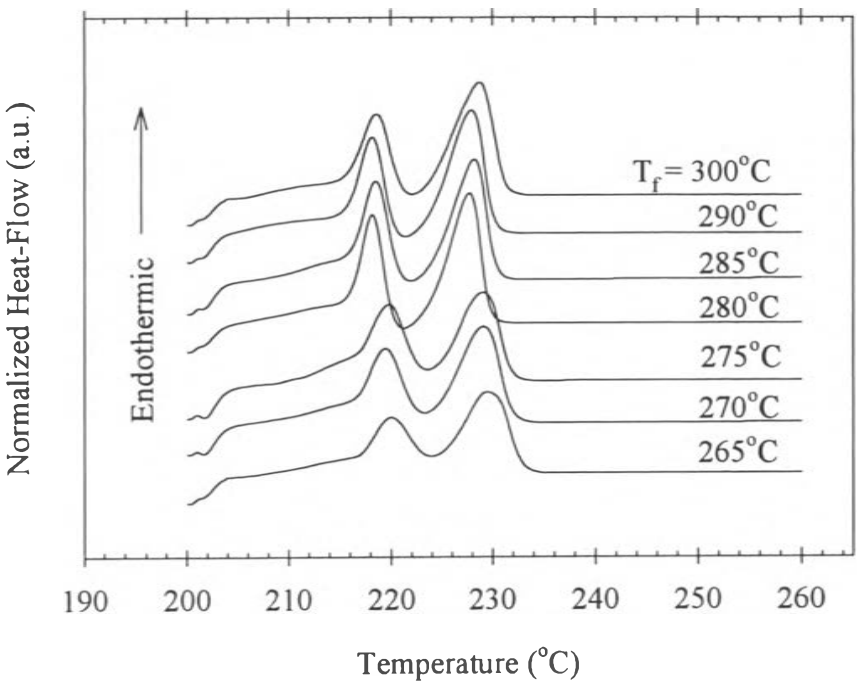
Normalized Heat-Flow (a.u.)
Endothermic
T_f = 300°C
290°C
285°C
280°C
275°C
270°C
265°C
190
200
210
220
230
240
250
260
Temperature (°C)

Figure 12

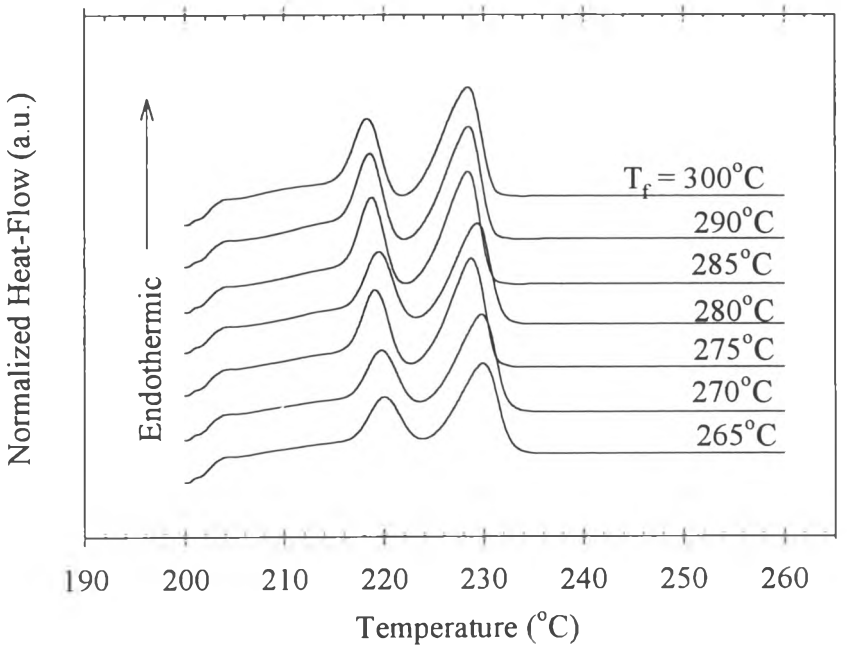
Normalized Heat-Flow (a.u.)
Endothermic
T_f = 300°C
290°C
285°C
280°C
275°C
270°C
265°C
190
200
210
220
230
240
250
260
Temperature (°C)

Figure 13